Chapter 3

Quinoxaline-2-carboxalidine-2-amino-5-methylphenol complexes of manganese(II), iron(III), cobalt(II), nickel(II), copper(II) and zinc(II)

Contents

3.1 INTRODUCTION

Multidentate ligands are extensively used for the preparation of metal complexes with interesting properties. Among these ligands, Schiff bases containing nitrogen and phenolic oxygen donor atoms are of considerable interest due to their potential application in catalysis, medicine and material science [1–4]. They have proven to be effective in constructing supramolecular architectures such as coordination polymers and helical assemblies [5–8]. Transition metal complexes of these ligands exhibit varying configurations, structural lability and sensitivity to molecular environments. The central metal ions in these complexes act as active sites for catalyzing chemical reactions. This feature is employed for modeling active sites in biological systems.

Aminophenols are important to the pharmaceutical industry, since they have antibacterial and antitubercular action. Schiff bases obtained by the condensation of 2-aminophenol with some aldehydes/ketones find application as antituberculosis compounds. They also find application in the biophysical and

clinical studies as metal ligand luminescence probes [9]. Recently light-emitting devices (LEDs) based on the small molecule like aminophenols were demonstrated [10]. There are a number of reports regarding Schiff base formation between aminophenol and salicylaldehyde derivatives [11-13]. However there is only one report on the Schiff base derived from aminophenol and quinoxaline-2-carboxaldehyde. The synthesis and characterization of quinoxaline-2-carboxalidine-2-aminophenol and its transition metal complexes have been reported by our group [14].

Therefore, in view of our interest in synthesis of new Schiff base complexes, which might find application as catalysts and as luminescence probes, we have synthesized and characterized new transition metal complexes of tridentate ONN donor Schiff base formed by the condensation of quinoxaline-2-carboxaldehyde and 2-amino-5-methylphenol. The results of our studies are presented in this chapter.

3.2 EXPERIMENTAL

3.2.1 Materials and methods

Synthetic procedure of quinoxaline-2-carboxaldehyde and the techniques employed for the characterization of ligand and complexes are given in chapter II.

3.2.2 Synthesis of quinoxaline–2–carboxalidine–2–amino–5–methylphenol (qamp)

The Schiff base quinoxaline–2–carboxalidine–2–amino–5–methylphenol (qamp) was synthesized by the reaction of quinoxaline–2–carboxaldehyde (10 mmol, 1.581 g) in methanol (60 mL) and 2–amino–5–methylphenol (10 mmol, 1.231 g) in methanol (20 mL). The solution was stirred for 3 hours. The yellow precipitate obtained was filtered, and was recrystallised from alcohol (Yield: 90 %, M.P.: 225 ºC).

3.2.3 Preparation of Complexes

The complexes of Mn(II), Fe(III), Co(II), Ni(II), Cu(II) and Zn(II) were prepared by the following procedure:

The Schiff base qamp (0.01 mol, 2.633 g) in 1:1 chloroform–methanol (50 mL) solution was added to a solution of manganese(II) acetate tetrahydrate (0.01 mol, 2.4510 g), ferric chloride (0.01 mol, 1.622 g), cobalt(II) acetate hexahydrate (0.005 mol, 1.245 g), nickel(II) acetate hexahydrate (0.005 mol, 1.244 g), copper(II) chloride dihydrate (0.01 mol, 1.705 g) or zinc(II)acetate dihydrate (0.005 mol, 1.097 g) in methanol (15 mL). The solution was then refluxed for three hours and left to cool at room temperature (28±2 °C) overnight. The crystalline complex separated out was filtered, washed with ether and dried in vacuum over anhydrous calcium chloride.

3.3 RESULTS AND DISCUSSION

The complexes are found to be stable in air and non-hygroscopic. They are soluble in common solvents like ethanol, methanol, acetonitrile and DMF. The analytical data (Table 3.1) show that the found and calculated values of the percentage of elements are in good agreement. The Co(II), Ni(II) and Zn(II) complexes are formed with metal to ligand ratio of 1:2. Other complexes are formed in 1:1 ratio. The very low conductance values (Table 3.2) of the complexes in DMF indicate the non-electrolytic nature of the complexes [15].

Table 3.1: ***Analytical data of qamp and its complexes***

Compound	Colour	Yield (%)	Analytical data. Found (calculated)%				
			C	H	N	M	Cl
qamp	Yellow	90	72.46 (72.99)	4.21 (4.98)	15.64 (15.96)	–	–
$[Mn(qamp)(OAc)].H_2O$	red	65	54.78 (54.83)	3.98 (4.35)	10.69 (10.66)	13.96 (13.93)	–
$[Fe(qamp)Cl_2]$	black	70	49.67 (49.40)	3.15 (3.11)	10.69 (10.80)	14.31 (14.35)	18.51 (18.23)
$[Co(qamp)_2].H_2O$	Violet	85	63.73 (63.90)	4.23 (4.36)	14.24 (13.97)	9.75 (9.80)	–
$[Ni(qamp)_2].H_2O$	blue	80	63.70 (63.92)	3.99 (4.36)	13.93 (13.98)	9.76 (9.74)	–
[Cu(qamp)Cl]	Violet	70	53.19 (53.16)	3.36 (3.35)	11.67 (11.63)	17.64 (17.59)	9.86 (9.81)
$[Zn(qamp)_2].2H_2O$	Violet	85	61.75 (61.40)	4.12 (4.51)	13.79 (13.42)	10.42 (10.45)	–

Table 3.2: ***Conductivity and magnetic moment data of complexes***

Compound	$\lambda_m^{\#}$	μ_{eff} (B.M)
$[Mn(qamp)(OAc)].H_2O$	15	5.94
$[Fe(qamp)Cl_2]$	9	4.01
$[Co(qamp)_2].H_2O$	4	5.08
$[Ni(qamp)_2].H_2O$	12	3.20
[Cu(qamp)Cl]	13	1.95
$[Zn(qamp)_2].2H_2O$	8	–

$^{\#}$ Molar conductivity (in Mho cm^2 mol^{-1}), 10^{-3} Molar solution in DMF

3.3.1 ^{1}H NMR spectra of the qamp and [Zn(qamp)$_2$].2H$_2$O

The proton NMR spectrum of the Schiff base (in $CDCl_3$) and that of the Zn(II) complex (in DMSO-d_6) were recorded using tetramethylsilane as the internal standard. The NMR spectrum of qamp is given in Figure 3.1 and the spectral data are summarized in Table 3.3. The signal at 9.70 ppm corresponds to phenolic –OH proton. The azomethine proton appears as a singlet at 8.98 ppm and all the eight aromatic protons appear as a multiplet in the range 7.80- 8.20 ppm. Protons of the methyl group attached to the phenolic ring resonate at 2.37 ppm as a singlet.

The NMR spectrum of the zinc(II) complex is given in Figure 3.2. The phenolic OH signal at 9.70 ppm observed in the spectrum of the ligand is not seen in the spectrum of the Zn(II) complex indicating the participation of the phenolic OH group in chelation with proton displacement. The signal due to azomethine proton gets shifted upon complexation, which might probably be due to the donation of the lone pair of electrons by the nitrogen to the central metal atom, resulting in the formation of a coordinate linkage (M ← N). The aromatic and quinoxaline protons resonate as a number of complex multiplets in the region δ 7.46–8.20 ppm. The signal due to methyl group attached to the phenolic ring is observed almost at the same chemical shift for that in spectrum of the ligand. A broad singlet appeared in the region 3.91– 4.26 indicates the presence of water molecules in the complex.

Table 3.3: ***^{1}H NMR Spectroscopic data of qamp and [Zn(qamp)$_2$].2H$_2$O***

Compound	Chemical shift, δ (ppm)	Assignment
qamp	9.70	(s, 1H, OH phenolic)
	8.98	(s, 1H, CH azomethine)
	6.80-8.20	(m, 8H, Ar)
	2.37	(s, 3H, methyl)
[Zn(qamp)$_2$].2H$_2$O	9.10	(s, 2H, CH azomethine)
	7.16-8.20	(m, 14H, Ar)
	2.40	(s, 6H, methyl)
	3.91-4.26	(br s, 4H, water)

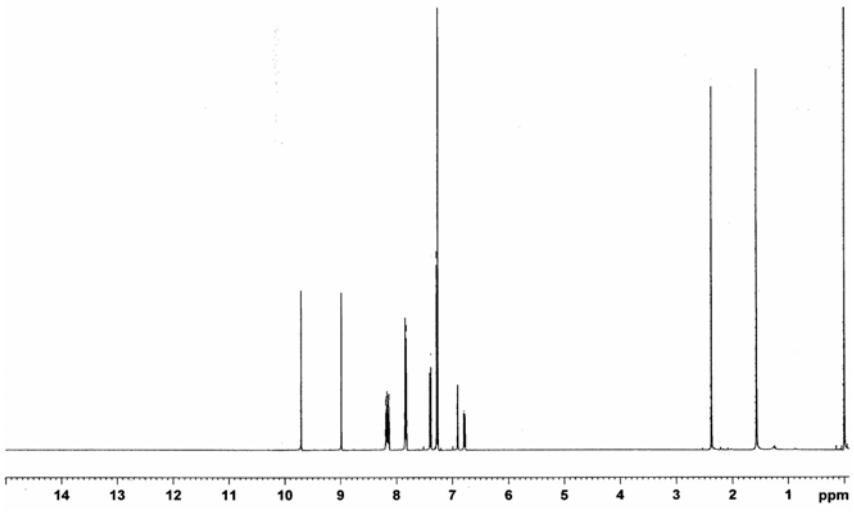

Figure 3.1: ***The ^{1}H NMR spectrum of qamp***

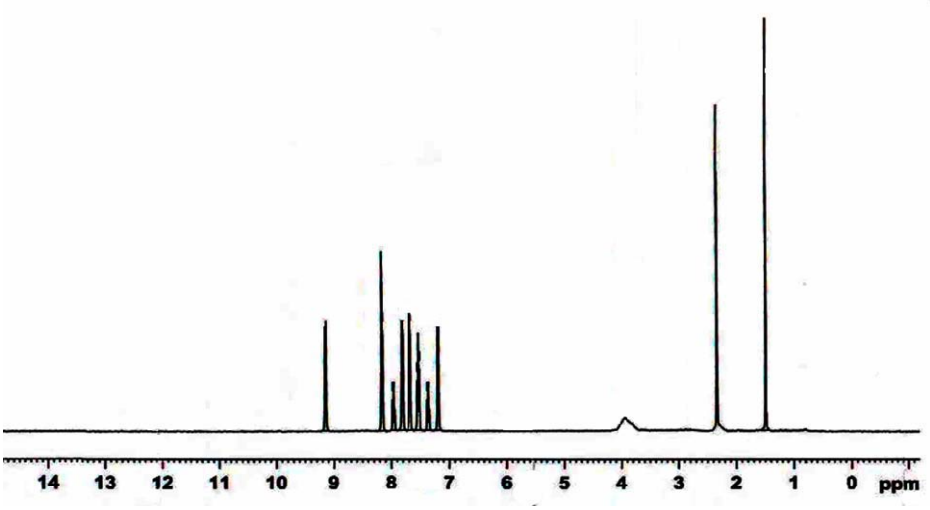

Figure 3.2: ***The ^{1}H NMR spectrum of $[Zn(qamp)_2].2H_2O$***

3.3.2 Magnetic susceptibility measurements

The magnetic moment values (at 28 ± 2 °C) of the complexes are shown in Table 3.2. The μ_{eff} value of the Mn(II) complex was found to be 5.94 B.M. as expected for high spin d^5 system. Iron(III) is known to exist in three states: high spin state with S=5/2 (ground term ^{6}A, μ =5.92 B.M.), intermediate spin state with S= 3/2 (ground term $^{4}A_2$, μ = 4.00 B.M) and the low spin state with S=1/2 (ground term $^{2}T_2$, μ = 2 to 2.6 B.M). The iron(III) complex shows a magnetic moment of 4.01 B.M., which confirms that iron(III) complex is five coordinated with the

intermediate spin state of 3/2 [16, 17]. The cobalt(II) complex exhibits a magnetic moment of 5.08 B.M. and the high magnetic moment value suggests an octahedral geometry for the complex. The nickel(II) complex has a magnetic moment value of 3.10 B.M., which is in the normal range observed for octahedral Ni(II) complexes [18]. The magnetic moment of the copper(II) complex is 1.95 B.M. which suggests the lack of Cu–Cu interactions and monomeric nature of the complex.

3.3.3 Infrared spectra

The most significant IR spectral bands along with their tentative assignments are listed in Table 3.4. The IR spectrum of the ligand is compared with that of the complexes to know the changes during complex formation.

On complexation the ν(C=N) band at 1626 cm^{-1} of the Schiff base shifts to lower or higher frequencies in the spectra of all the complexes indicating coordination of the azomethine nitrogen [19]. For the Schiff base, the C=N– stretching of quinoxaline ring is observed as a strong band at 1577 cm^{-1}. This band undergoes a small shift (~5 cm^{-1}) on complexation; such small shifts have been reported when ring nitrogens are involved in coordination to the metal [20]. The ν(C–O) band for all the complexes appears at lower frequencies compared to that for the free ligand, suggesting the deprotonation and coordination of phenolic oxygen [21]. Thus the Schiff base coordinates through azomethine nitrogen, phenolic oxygen and quinoxaline oxygen and acts as a monobasic tridentate ligand (Figure 3.3).

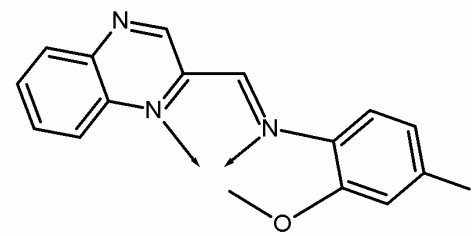

Figure 3.3: ***Mode of coordination of qamp***

The manganese(II), cobalt(II), nickel(II) and the zinc(II) complexes exhibit a broad band in the region 3300–3400 cm^{-1} due to the presence of water molecule. Appearance of new bands in the spectra of all the complexes (Figures 3.4-3.10) in the regions 490–450 and 450–400 cm^{-1} has been attributed to ν(M–O) and ν(M–N), respectively. The IR spectrum of the acetato complex, [MnL(OAc)].H_2O, displays ν_{asym} (COO^-) and ν_{sym} (COO^-) at 1545 and 1390 cm^{-1} suggesting monodentate acetato coordination [22].

Table 3.4: ***IR spectral data of qamp and its complexes***

Assignments (in cm^{-1})	ν (OH)	ν (C=N) #	ν (C=N) *	ν (C–O) $	ν (M–O)	ν (M–N)
qamp	3330	1626	1577	1261	-	-
[Mn(qamp)(OAc)].H_2O	3300 b	1606	1584	1234	465	413
[Fe(qamp)Cl_2]	-	1583	1547	1255	490	424
[Co(qamp)$_2$].H_2O	3390	1664	1579	1252	567	468
[Ni(qamp)$_2$].H_2O	3200b	1674	1579	1254	457	432
[Cu(qamp)Cl]	-	1612	1578	1252	425	409
[Zn(qamp)$_2$].$2H_2O$	3381	1672	1587	1252	465	418

b-broad, # azomethine, * quinoxaline, $ phenolic

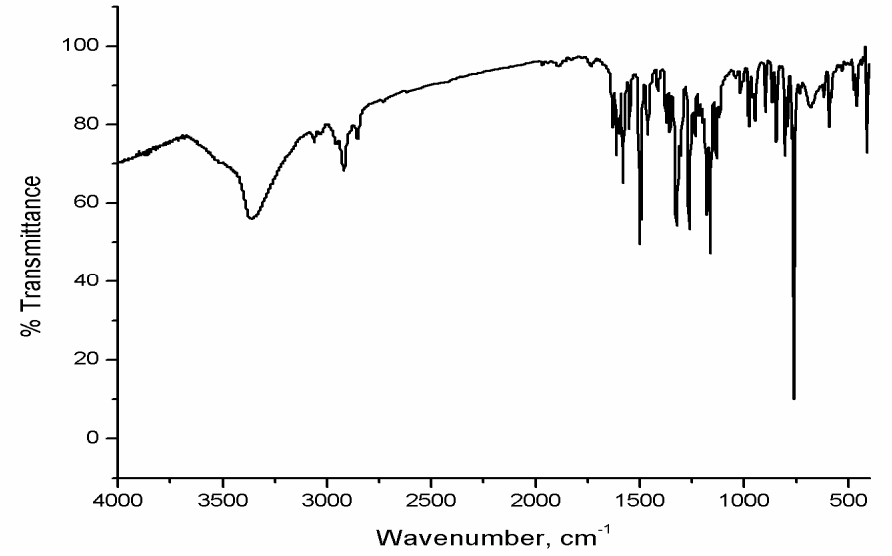

Figure 3.4: ***FTIR spectrum of the Schiff base qamp***

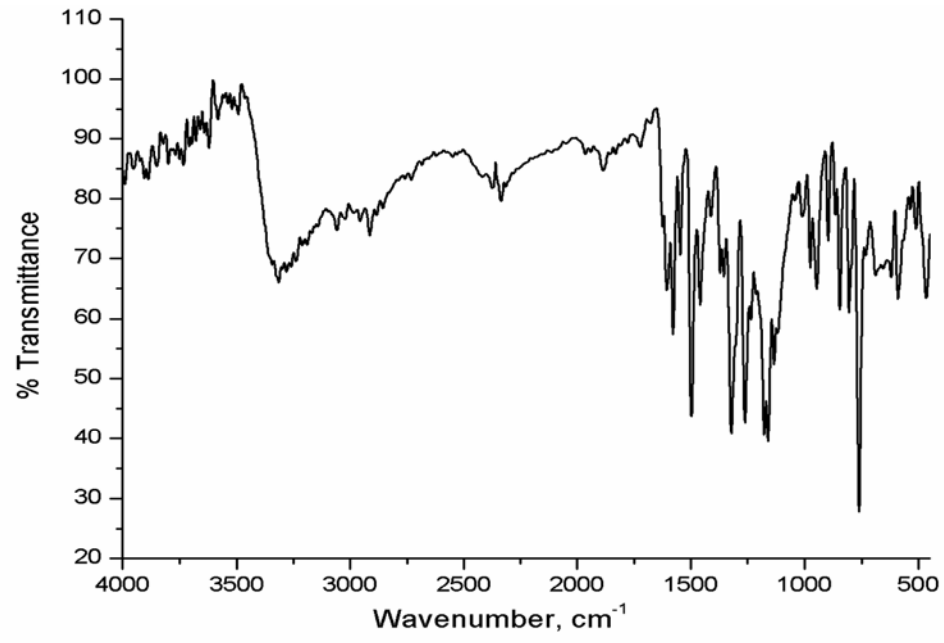

Figure 3.5: ***FTIR spectrum of [Mn(qamp)(OAc)].H_2O***

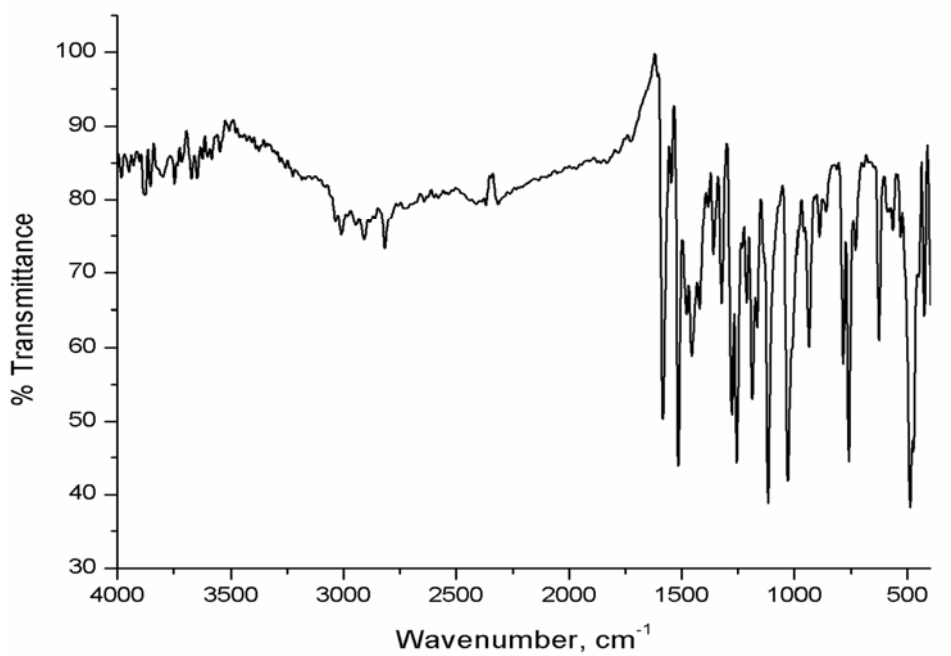

Figure 3.6: ***FTIR spectrum of [Fe(qamp)Cl_2]***

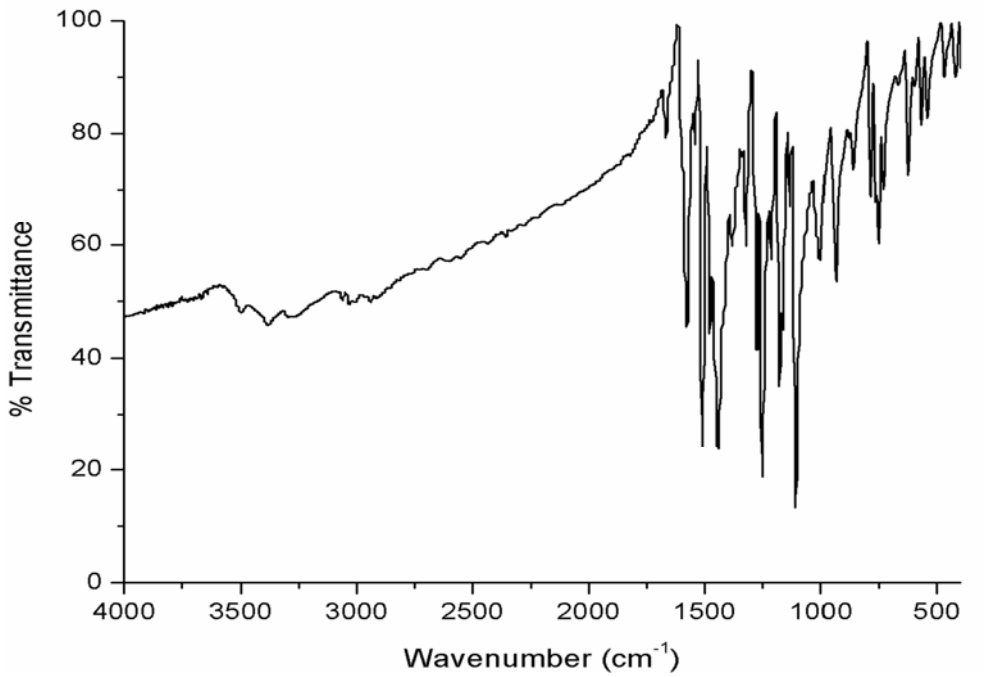

Figure 3.7: ***FTIR spectrum of [Co(qamp)$_2$].H$_2$O***

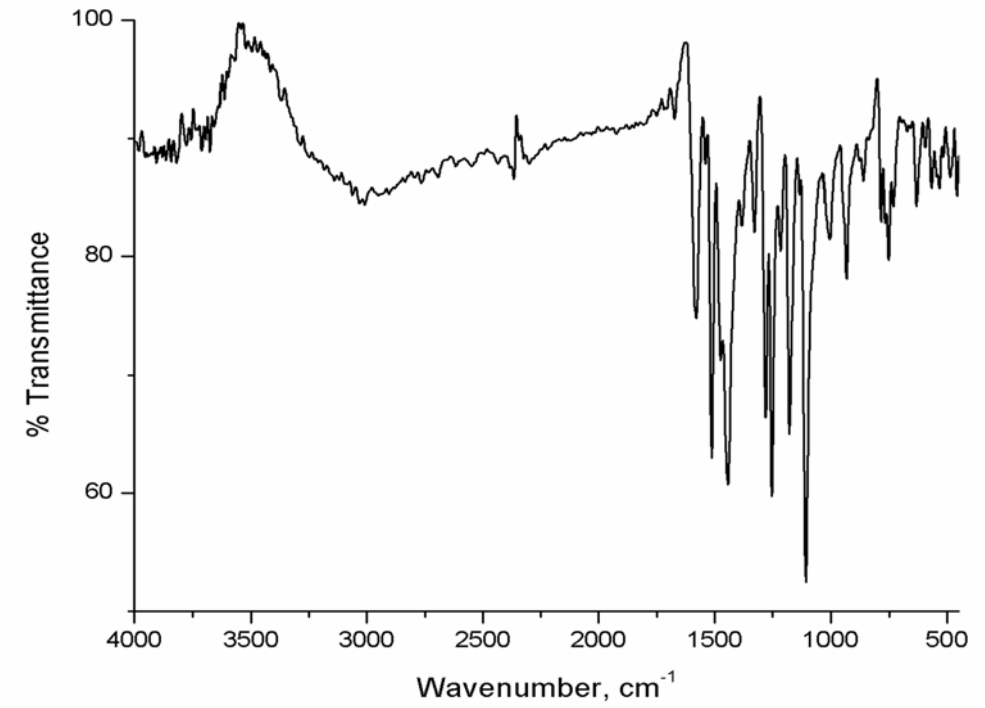

Figure 3.8: ***FTIR spectrum of [Ni(qamp)$_2$].H$_2$O***

Figure 3.9: ***FTIR spectrum of [Cu(qamp)Cl]***

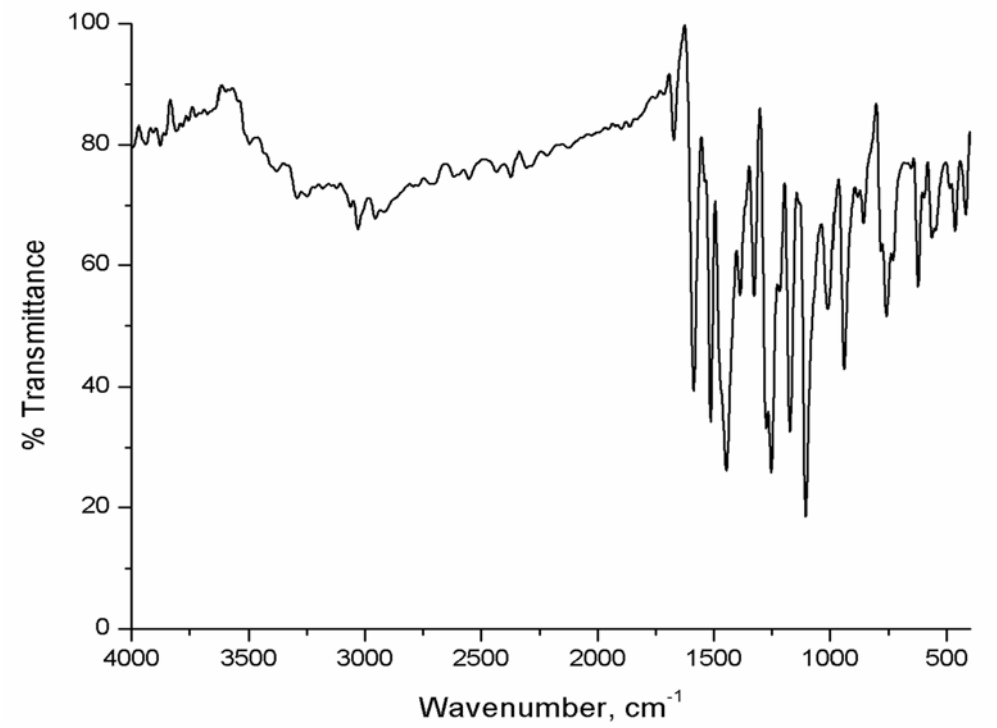

Figure 3.10: ***FTIR spectrum of [Zn(qamp)$_2$].2H$_2$O***

3.3.4 Electronic spectra

Electronic spectra of the Schiff base and its complexes were taken in methanol (~5x10^{-4} molar) in the range 50000-10000 cm^{-1}. The absorption maxima are listed in the Table 3.5 and the spectra are given in Figure 3.11-3.17. The UV–Vis spectrum of the Schiff base shows two strong bands at 42500 and 26000 cm^{-1} due to π–π* transitions [23]. These π–π* bands are not altered to a greater extent on complexation.

The spectrum of the Mn(II) complex shows two shoulders at 10810 and 9300 cm^{-1} assignable to $^6A_1 \rightarrow {}^4T_1$ and $^6A_1 \rightarrow {}^4T_2$ (G) transitions respectively [24, 18].

The solution state electronic spectrum of the iron(III) complex did not show any d-d bands. Two charge transfer bands are seen at 24000 and 18200 cm^{-1} respectively. Since the solution spectrum does not give information regarding geometry probably due to the limited solubility of the complex in methanol, we have taken the spectrum in nujol mull (Figure 3.18). The d-d bands are seen in the solid state spectra due to the high concentration of the complex in the solid state. Two bands are seen in the visible region at 11110 and 10200 cm^{-1}, and a weak broad band is observed in the near IR region at 6890 cm^{-1} indicating a square pyramidal structure. Similar observations have been made by Martin and White for the five coordinated iron(III) dithiocarbamate complex [25, 26].

For the cobalt(II) complex, a band with maxima at 18550 cm^{-1} is due to the $^4T_{1g}(F) \rightarrow {}^4T_{2g}(P)$ transition [25]. The intensities of the d–d band is considerably increased possibly due to the influence of nearby intense charge-transfer transitions (log ε = 3.36). The other d–d transitions are masked by the strong charge transfer band, as has been observed in the case of similar Schiff base complexes [27, 28].

For the nickel(II) complex, the band at 17450 cm^{-1} is due to the $^3A_{2g} \rightarrow {}^3T_{1g}$ transition of nickel(II) in octahedral environment. The intensity of this d–d band is

also considerably increased possibly due to the influence of nearby intense charge-transfer transitions [25].

The spectrum of [Cu(qamp)Cl] shows bands at 22220 and 16000 cm^{-1} assignable to $^2B_{1g}\rightarrow{}^2A_{1g}$ and $^2B_{1g}\rightarrow{}^2E_g$ transitions, respectively [25,29] as expected for the square planar copper(II) complexes. The zinc(II) complex exhibits a charge transfer transitions at 18310 cm^{-1}.

Table 3.5: ***Electronic spectral data (in methanol)***

Compound	Absorption maxima (cm^{-1})	log ε (ε in L mol^{-1} cm^{-1})	Tentative assignments
qamp	42500	3.96	$\pi\rightarrow\pi^*$
	26000	3.81	$\pi\rightarrow\pi^*$
[Mn(qamp)(OAc)].H_2O	41320	3.56	$\pi\rightarrow\pi^*$
	29850	3.25	$\pi\rightarrow\pi^*$
	26400	3.30	CT
	18280	3.27	CT
	10800	1.67	$^6A_1\rightarrow{}^4T_1$
	9300	1.68	$^6A_1\rightarrow{}^4T_2(G)$
[Fe(qamp)Cl_2]	42920	4.12	$\pi\rightarrow\pi^*$
	24000	3.96	CT
	18200	3.70	CT
[Co(qamp)$_2$].H_2O	41850	3.62	$\pi\rightarrow\pi^*$
	29400	3.32	$\pi\rightarrow\pi^*$
	26450	3.35	$n\rightarrow\pi^*$
	18550	3.36	$^4T_{1g}(F)\rightarrow{}^4T_{1g}(P)$
[Ni(qamp)$_2$].H_2O	41150	4.13	$\pi\rightarrow\pi^*$
	27850	3.88	$\pi\rightarrow\pi^*$
	17450	3.83	$^3A_{2g}\rightarrow{}^3T_{1g}$
[Cu(qamp)Cl]	40320	3.74	$\pi\rightarrow\pi^*$
	33900	2.44	$n\rightarrow\pi^*$
	28490	3.65	CT
	22220	2.08	$^2B_{1g}\rightarrow{}^2A_{1g}$
	16000	1.97	$^2B_{1g}\rightarrow{}^2E_g$
[Zn(qamp)$_2$].$2H_2O$	42200	3.72	$\pi\rightarrow\pi^*$
	30400	3.30	$\pi\rightarrow\pi^*$
	25840	3.31	$\pi\rightarrow\pi^*$
	18310	3.36	CT

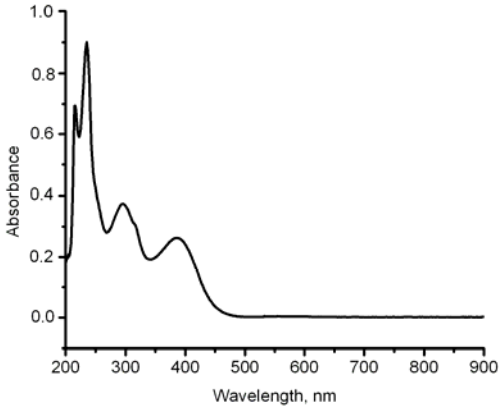

Figure 3.11: ***The UV-Vis spectrum of qamp***

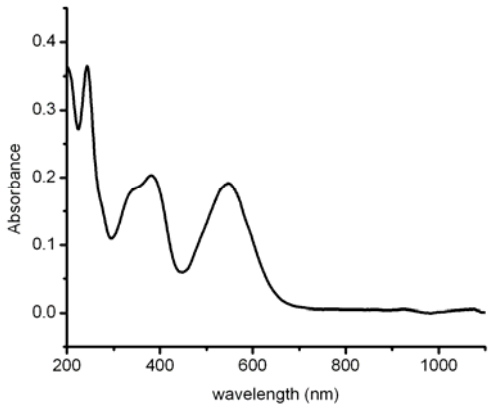

Figure 3.12: ***The UV-Vis spectrum of [Mn(qamp)(OAc)].H_2O***

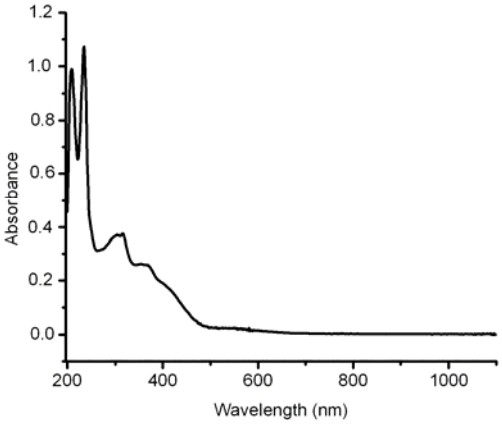

Figure 3.13: ***The UV-Vis spectrum of [Fe(qamp)Cl_2]***

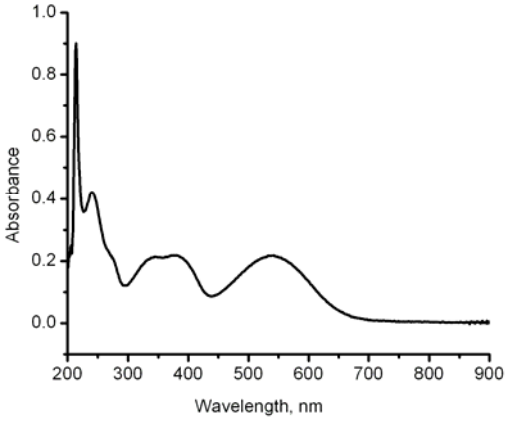

Figure 3.14: ***The UV-Vis spectrum of [Co(qamp)$_2$].H_2O***

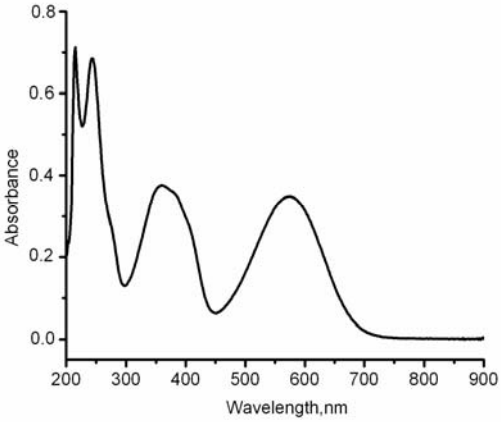

Figure 3.15: ***The UV-Vis spectrum of [Ni(qamp)$_2$].H_2O***

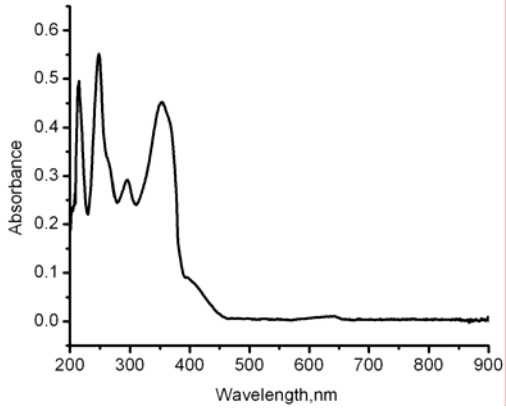

Figure 3.16: ***The UV-Vis spectrum of [Cu(qamp)Cl]***

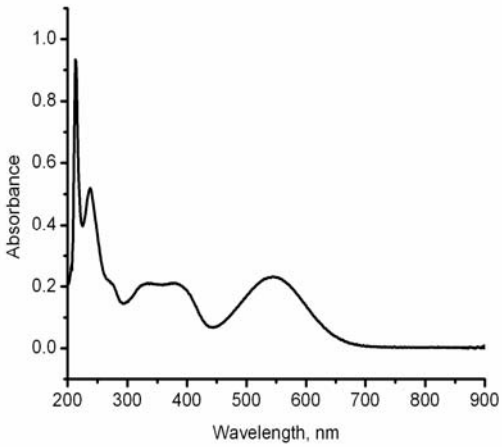

Figure 3.17: ***The UV-Vis spectrum of [Zn(qamp)$_2$].2H$_2$O***

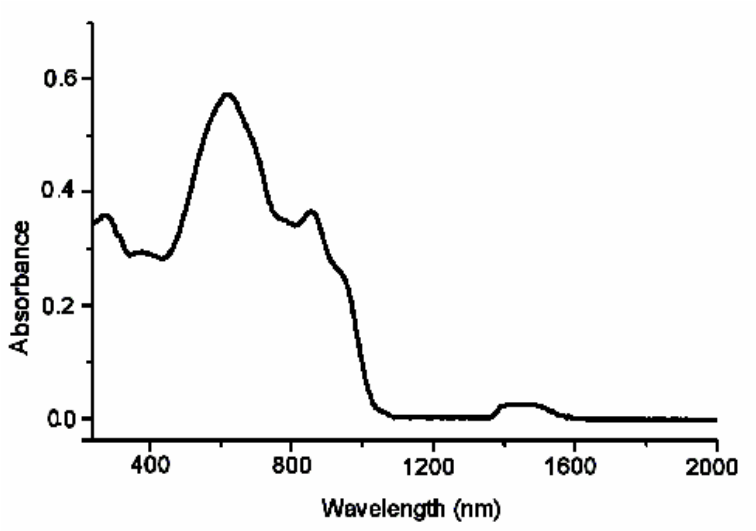

Figure 3.18: ***UV-Vis-NIR spectrum of [Fe(qamp)Cl$_2$] in nujol mull***

3.3.5 Thermal analysis

The TG DTG plots of the ligand and complexes are given in Figures 3.19-3.25. The Schiff base, qamp, exhibits a one stage decomposition which begins at 160 ºC. The weight loss observed for the Mn(II), Co(II), Ni(II) and Zn(II) complexes in the range 40-140 ºC is due to the removal of lattice water (Table 3.6). The TG data indicate the presence of one hydrated water molecule in the

manganese(II), cobalt(II) and nickel(II) complexes, and two water molecules in the zinc(II) complex. All the compounds are found to be thermally stable and exhibit multi stage decomposition pattern. TG results show good agreement with the molecular formula arrived from the analytical data.

Table 3.6: ***TG data of the complexes below 200℃***

Complex	Temperature Range, ºC	% loss	Fragment lost	Nature of water lost
[Mn(qamp)(OAc)].H_2O	46–101	4.5	1 H_2O	Lattice water
[Co(qamp)$_2$].H_2O	50–120	3.0	1 H_2O	Lattice water
[Ni(qamp)$_2$].H_2O	50–130	3.1	1 H_2O	Lattice water
[Zn(qamp)$_2$].2H_2O	70–140	2.9	1 H_2O	Lattice water

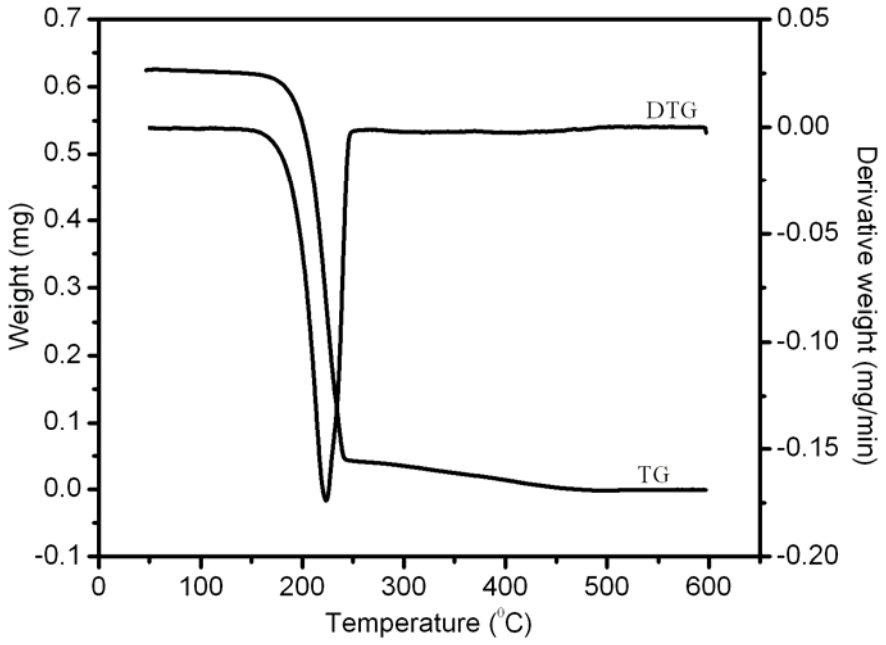

Figure 3.19: ***TG DTG of qamp***

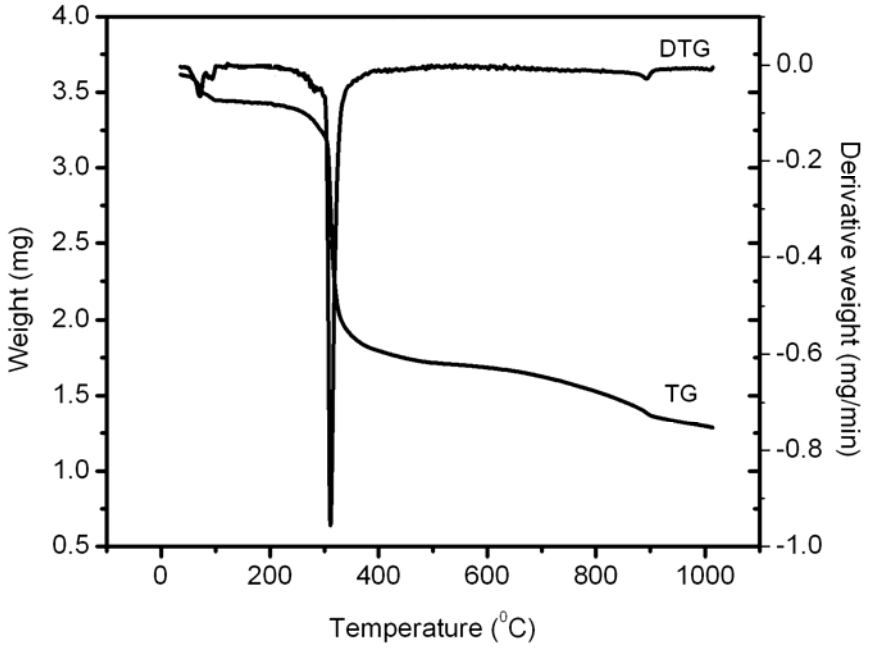

Figure 3.20: ***TG DTG of [Mn(qamp)(OAc)].H_2O***

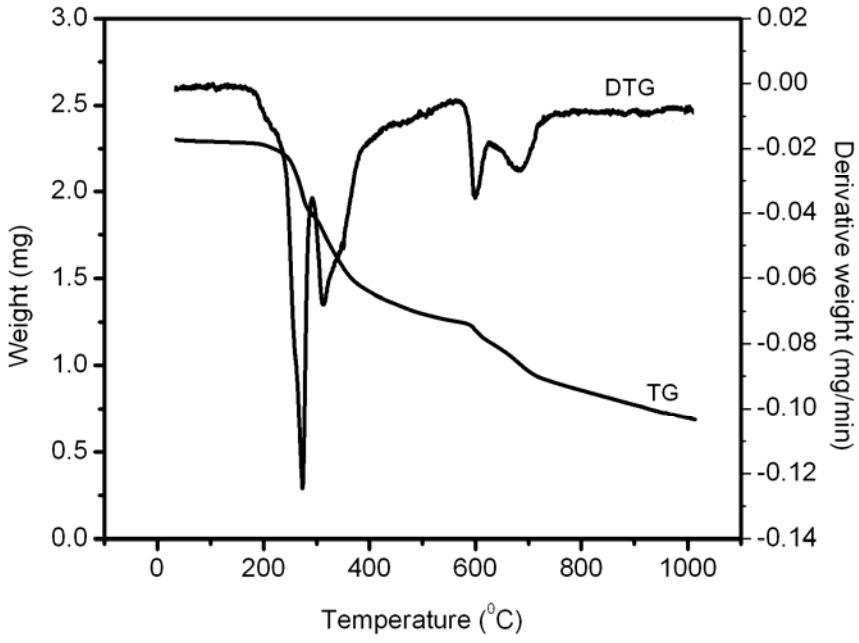

Figure 3.21: ***TG DTG of [Fe(qamp)Cl_2]***

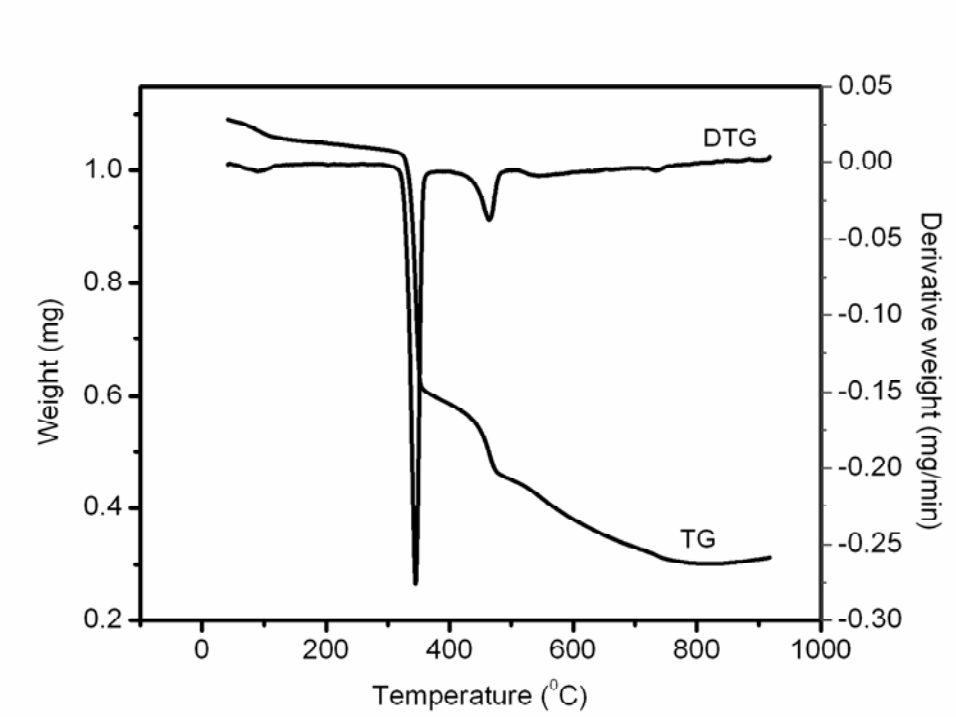

Figure 3.22: ***TG-DTG of [Co(qamp)$_2$].H$_2$O***

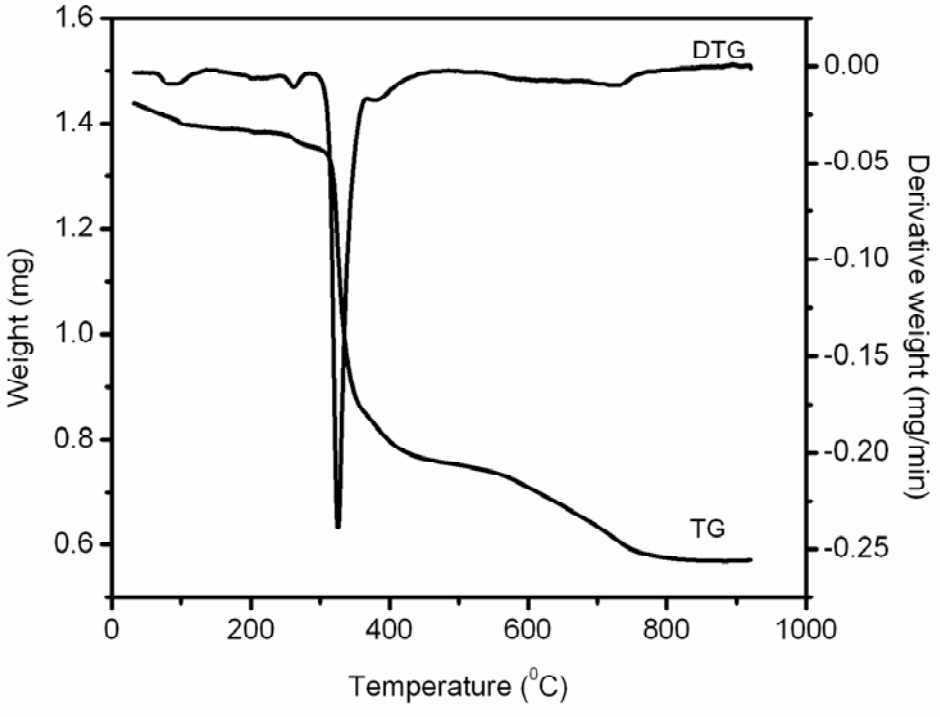

Figure 3.23: ***TG-DTG of [Ni(qamp)$_2$].H$_2$O***

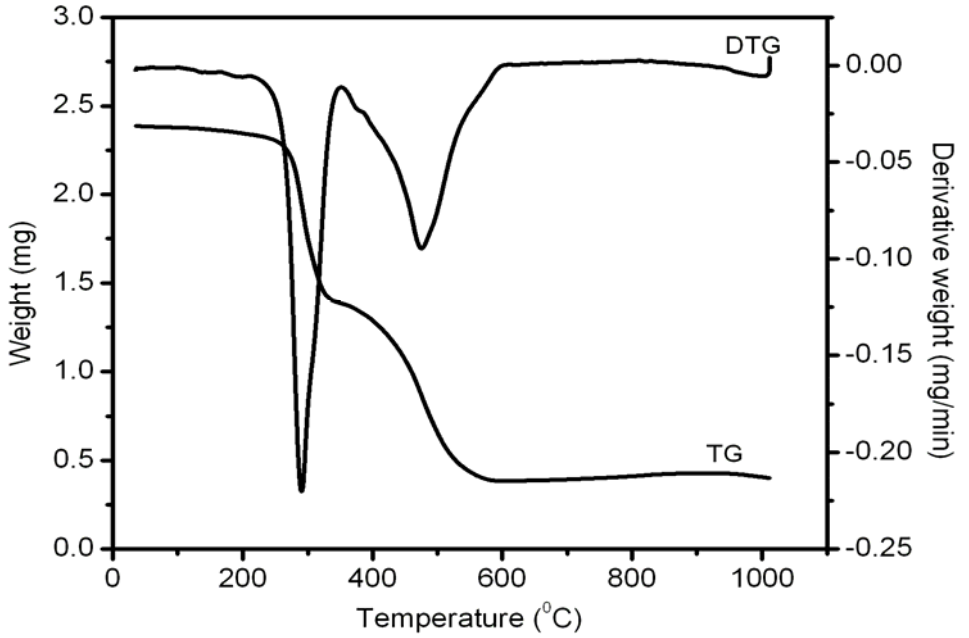

Figure 3.24*: TG-DTG of [Cu(qamp)Cl]*

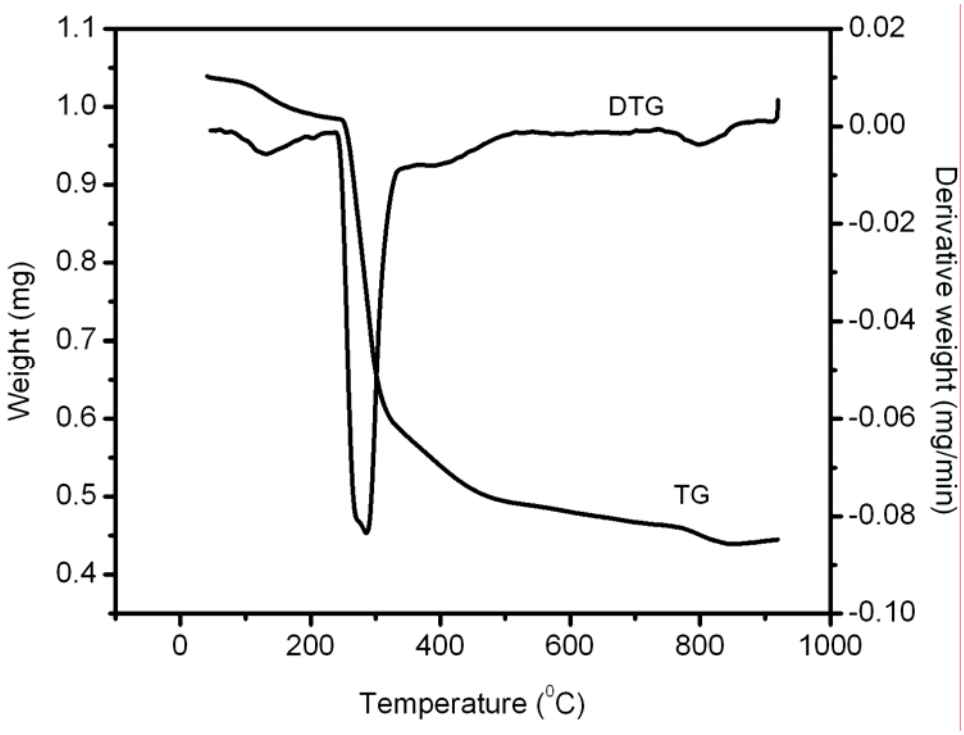

Figure 3.25*: TG-DTG of [Zn(qamp)$_2$].2H$_2$O*

3.3.6 EPR spectra

The X band EPR spectra of the manganese(II) complex is taken in polycrystalline state at 298 K and in DMSO at 77K (Figure 3.26). The spin Hamiltonian used to represent EPR spectra of Mn(II) is given by,

$\hat{H}=g\beta HS+D[S_z^2-S(S+1)/3]+E(S_x^2-S_y^2)$

where H is the magnetic field vector, g is the spectroscopic splitting factor , β is the Bohr magneton, D is the axial zero field splitting term, E is rhombic zero field splitting parameter and S is the electron spin vector [30]. If D and E are very small compared to $g\beta HS$, six EPR transitions are expected. The solid state EPR spectrum of the Mn(II) complex is characterized by the broad isotropic spectrum with a *g* value of 1.98. The solution spectrum gives six hyperfine lines with the spin forbidden transitions in between the lines. The spectrum gives a *g* value of 1.98 with an *A* value of 0.011 cm^{-1}.

The copper(II) ion, with a d^9 configuration, has an effective spin of S= 3/2 and is associated with a spin angular momentum m_s=1/2, leading to a doubly degenerate spin state in the absence of a magnetic field. In a magnetic field, this degeneracy is lifted and the energy difference between these states is given by $E=h\nu=g\beta H$ where *h* is the Planck's constant, ν is the frequency, *g* is the Landé splitting factor, β is the electronic Bohr magneton and *H* is the magnetic field. For $3d^9$ copper(II) ion the appropriate spin Hamiltonian assuming a B_{1g} ground state is given by [31]

$H=\beta[g_{\parallel}H_zS_z+g_{\perp}(H_xS_x+H_yS_y)]+AI_zS_z+B(I_xS_x+I_yS_y)$

The EPR spectrum of the copper(II) complex in polycrystalline state gives an isotropic spectrum with a *g* value of 1.98. This spectrum exhibits a broad signal which arises from extensive exchange coupling through misalignment of the local molecular axes between different molecules in the unit cell (dipolar broadening) and enhanced spin lattice relaxation. This type of spectra gives no information on the electronic ground state of the Cu(II) ion present in the complexes. The EPR spectrum of the copper(II) complex gives a spectrum with $g_{\|}$ and $g\perp$ values of 2.28 and 2.12 respectively (Figure 3.27). The trend $g_{\|} > g\perp > g_e$ observed for copper(II) complex shows that the unpaired electron is most likely localized in $d_{x^2-y^2}$ orbital of copper(II) ion and the spectral features are characteristic of an axial symmetry [32, 33].

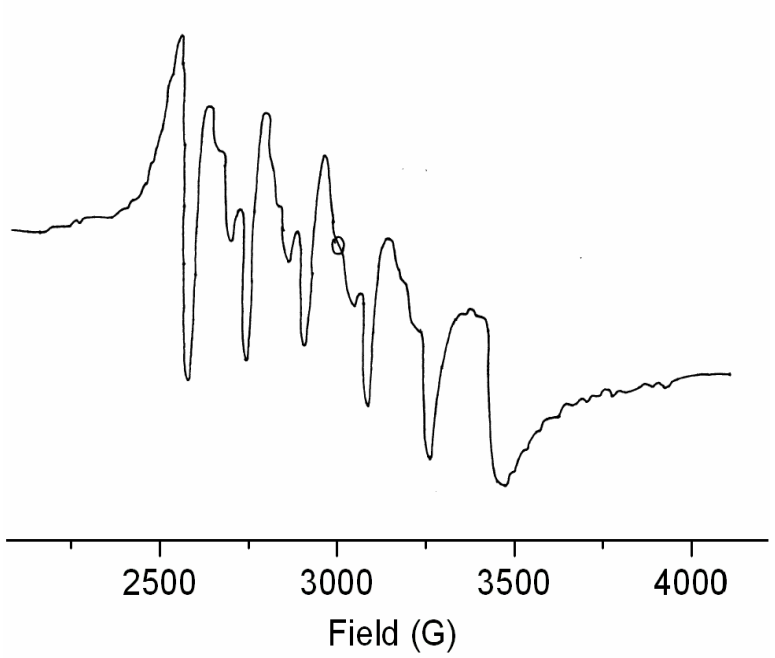

Figure 3.26: ***EPR spectrum of [Mn(qamp)(OAc)].H_2O at 77 K***

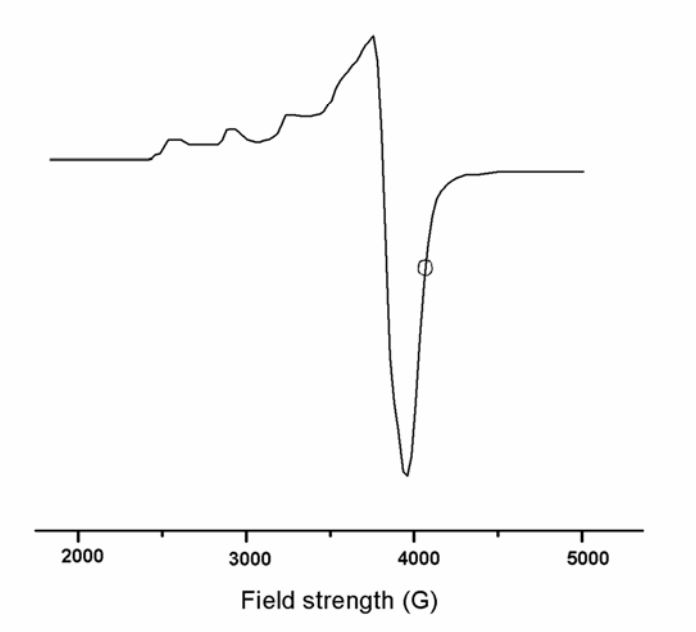

Figure 3.27: ***EPR spectrum of [Cu(qamp)Cl] at 77 K***

3.3.7 Crystal structure analysis

3.3.7.1 Crystal structure of cobalt(II) complex of quinoxaline-2-carboxalidine-2-amino-5-methylphenol

The single crystals suitable for XRD were obtained by the slow evaporation of methanolic solution of the complex. The geometry of the complex is found to be distorted octahedral with one lattice water molecule. The compound crystallises in monoclinic crystal system with the space group $P2_1/n$. A summary of crystallographic data and refinement parameters are given in Table 3.7.

The molecular structure of the compound was solved at 298 K. Figure 3.28 gives the ORTEP diagram of the complex with atomic labelling scheme. The unit cell of the crystal contains four molecules of ($C_{32}H_{26}CoN_6O_3$). The important interatomic distances and angles are listed in Table 3.8. The phenolic hydroxyl group is deprotonated on complexation. Two of the monoanionic tridentate Schiff base ligands wrap the cobalt(II) center in the *cis* mode with coordination of two oxygen and four nitrogen atoms (N_4O_2) in a distorted octahedral geometry.

Table 3.7: ***Crystal data summary for [Co(qamp)$_2$].H$_2$O***

Empirical formula	$C_{32}H_{26}CoN_6O_3$
Formula weight	601.52
Crystal size (mm^3)	0.40 x 0.36 x 0.02
Wavelength (Å)	0.71073
Crystal system	Monoclinic
Space group	$P2_1/n$
Cell constants:	
Unit cell and dimensions (Å)	
a (Å)	13.7959(15)
b (Å)	13.8622(15)
c (Å)	14.5161(16)
β(º)	94.684(2)
V ($Å^3$)	2766.8(5)
Z	4
D_{calcd} (gcm^{-3})	1.444
Absorption coefficient (mm^{-1})	0.666
F(000)	1244
θ range for data collection (º)	1.96 to 26.03
Reflections collected / unique	27217 / 5445 [R(int) = 0.0841]
Max. and min. transmission	0.987 and 0.766
Data / restraints / parameters	5416 / 0 / 391
Goodness-of-fit on F^2	1.205
R_1 , wR_2 [I > 2sigma(I)]	0.0975, 0.1807
R_1 , wR_2 (all data)	0.1283, 0.1940

$R_1 = \sum (|Fo| - |Fc|) / \sum |Fo|$, $wR_2 = [\sum w(Fo^2-Fc^2)^2 / \sum w(Fo^2)^2]^{0.5}$.

The azomethine (C=N) bond lengths (1.288(6) and 1.279(6) Å) are well within the range of theoretical value (~1.285 Å) [34]. The molecule has no symmetry elements other than a C2 symmetry axis and is expected to exhibit optical isomerism. However, both enantiomers coexist in the unit cell, making the space group centrosymmetric (Figure 3.29). The complex geometry can be explained by a rigid structure resulting in O(2)–Co(1)–N(5) and O(1)–Co(1)–N(2)

bond angles that deviate significantly from linearity, i.e. 153.46(15) and 155.61(15)°. In the coordination sphere, the Co–O bond lengths are 2.031(4) and 2.045(4) Å; Co–N bond lengths are 2.049(4), 2.052(4), 2.256(4), and 2.310(4) Å. The Co–N (quinoxaline) bonds are elongated compared to Co–N (azomethine) bonds probably due to rigidity of the Schiff base. The benzene rings of the symmetry related quinoxalines are stacked via π–π interactions, having a centroid to centroid distance of 3.532 Å. Molecules are held together by O(3)–H(2)–N(3) and O(3)–H(31)–O(2) intermolecular hydrogen bonding and weak inter and intramolecular hydrogen bonding (Table 3.9) forming a 2-D polymeric structure parallel to the [010] plane as shown in Figure 3.30.

Table 3.8: ***Selected bond lengths and angles for [Co(qamp)$_2$].H$_2$O***

Bond lengths (Å)			
Co(1)–O(1)	2.031(4)	Co(1)–N(2)	2.257(4)
Co(1)–O(2)	2.044(4)	Co(1)–N(5)	2.310(4)
Co(1)–N(4)	2.049(4)	N(1)–C(8)	1.288(6)
Co(1)–N(1)	2.052(4)	N(4)–C(24)	1.279(6)
Bond angles (º)			
O(1)–Co(1)–O(2)	100.56(18)	O(2)–Co(1)–N(5)	153.47(15)
O(1)–Co(1)–N(4)	96.56(15)	N(4)–Co(1)–N(5)	74.89(16)
O(2)–Co(1)–N(4)	79.73(15)	N(1)–Co(1)–N(5)	106.10(15)
O(1)–Co(1)–N(1)	80.00(16)	N(2)–Co(1)–N(5)	92.48(14)
O(2)–Co(1)–N(1)	99.71(15)	C(1)–O(1)–Co(1)	112.9(3)
N(4)–Co(1)–N(1)	176.38(17)	C(17)–O(2)–Co(1)	112.9(3)
O(1)–Co(1)–N(2)	155.63(15)	C(8)–N(1)–Co(1)	118.7(4)
O(2)–Co(1)–N(2)	87.80(15)	C(2)–N(1)–Co(1)	113.3(3)
N(4)–Co(1)–N(2)	107.49(16)	C(24)–N(4)–C(18)	126.3(4)
N(1)–Co(1)–N(2)	76.02(16)	C(24)–N(4)–Co(1)	120.3(4)
O(1)–Co(1)–N(5)	89.99(16)	C(18)–N(4)–Co(1)	113.4(3)

Table 3.9: ***Selected hydrogen bond interactions in the complex***

D-H...A	Symmetry	Distances (Å)		Angles (◦)
		D...A	H...A	D-H...A
O(3)-H(2)...N(3)	1/2+x, 3/2-y, -1/2+z	3.035(10)	2.51(8)	124(6)
O(3)–H(31)...O(2)	1–x, 1–y, 1–z	2.895(9)	2.01(8)	169(6)

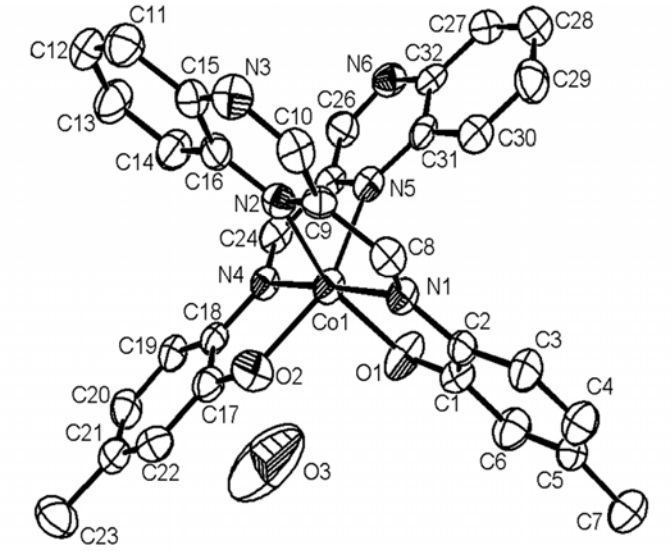

Figure 3.28: ***ORTEP diagram of [Co(qamp)$_2$].H$_2$O showing the atom labeling scheme with 50% probability ellipsoids.***

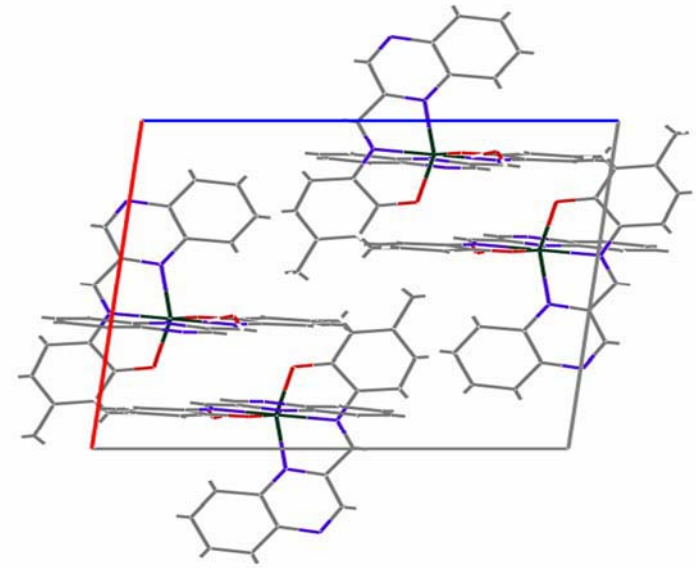

Figure 3.29: ***Unit cell packing of the complex along b axis***

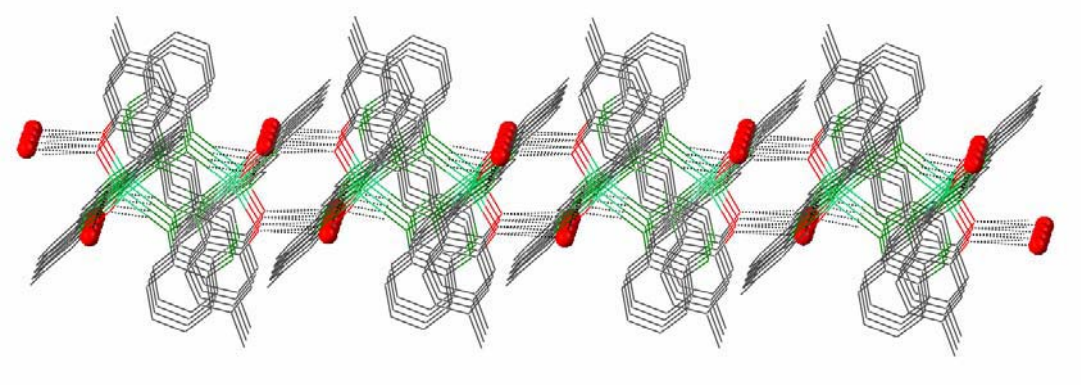

Figure 3.30: ***Two dimensional structure of [Co(qamp)$_2$].H$_2$O***

3.3.7.2 Crystal structure of nickel(II) complex of quinoxaline-2-carboxalidine-2-amino-5-methylphenol

The single crystals suitable for XRD were obtained by the slow evaporation of methanolic solution of the complex. The compound crystallises in monoclinic crystal system with the space group $P2_1/n$. A summary of crystallographic data and refinement parameters are given in Table 3.10.

Single crystal X-ray diffraction analysis reveals that the nickel(II) complex forms a two-dimensional polymeric chain due to the aggregation of the discrete monomeric entities through classical intermolecular O–H…O and O–H…N hydrogen bonds. The asymmetric unit as illustrated in the ORTEP diagram (Figure 3.31), consists of a monomeric Ni{$(CH_3)C_6H_4(O)N{=}CH{-}C_8H_5N_2$}$_2$ unit with a solvent water molecule present in the lattice. In the complex, the ligand quinoxaline –2–carboxalidine–2–amino–5–methyl phenol behaves as a monoanionic, tridentate Schiff base with its NNO donor set which coordinates to the metal center through one imine nitrogen, one quinoxaline ring nitrogen atom and a deprotonated phenolic oxygen atom in a mer arrangement. The nickel(II) center adopts a distorted octahedral geometry being chelated by two units of such tridentate Schiff base ligands.

Selected bond lengths and angles are listed in Table 3.11. The Ni–N(imine) distances are comparable to those observed for the similar kind of complexes

present in the literature [35, 36, 47]. The three trans-angles at nickel(II) are 176.00(18), 157.68(16) and 159.61(17) º for N(3)–Ni(1)–N(6), O(1)–Ni(1)–N(1) and O(2)–Ni(1)–N(4) which shows slight variation from 180 º while the cis angles differ in the range 76.64(18)–106.03(17) which also deviates from the ideal value of 90 º. These deviations in bite angles are due to the rigid structure of the Schiff base.

Table 3.10: ***Crystal data summary for [Ni(qamp)$_2$].H$_2$O***

Formula	**C_{32} H_{26} Ni N_6 O_3**
Formula weight	601.30
Crystal system	Monoclinic
Space group	$P2_1/n$
a/Å	13.677(4)
b /Å	13.760(3)
c /Å	14.572(4)
β /º	96.445(5)
V /Å^3	2725.1(12)
Z	4
T(K)	298
Dc/mg m^{-3}	1.466
μ(Mo $K\alpha$)/mm^{-1}	0.76
F(000)	1248
θ range for data collection /º	1.94 to 25.00
Reflections collected / unique	12261 / 4797
Goodness-of-fit on F2	1.194
R1 , wR2 [I > 2sigma(I)]	0.0884, 0.1529
R1 , wR2 (all data)	0.1117, 0.1630

R1 = ∑ (|Fo| – |Fc|) / ∑ |Fo|, wR2 = [∑w(Fo2–Fc2)2/ ∑ w(Fo2)2]0.5.

A further insight into the structure of the complex reveals the presence of a C2 symmetry axis and is expected to exhibit optical isomerism. However both the enantiomers coexist in the unit cell, being the space group centro-symmetric [38]. Both hydrogen of the uncoordinated water molecule are involved in the intermolecular hydrogen bonding with the neighbouring phenolic oxygen atom and uncoordinated quinoxaline nitrogen atom through O(3)–H1w…N(5) and O(3)–H2w …O(1) interactions. Similarly there are some weak intermolecular and intramolecular hydrogen bondings in the lattice. There is π–π stacking interaction between phenolic ring and symmetry related quinoxaline. A few significant hydrogen bonding parameters are listed in Table 3.12. It makes the monomeric unit a good template which is an important factor in establishing an ordered supramolecular structure formed by self-assembly [39-43]. All these interactions afford an infinite two dimensional chain propagating along [010] direction which is similar to that of cobalt(II) complex of qamp (Figure 3.30).

Table 3.11: ***Selected bond lengths (Å) and angles (º) for [Ni(qamp)$_2$].H$_2$O***

Bond lengths			
Ni(1) –N(3)	1.988(4)	N(1) – C(1)	1.359(6)
Ni(1) – N(6)	1.992(4)	N(2) – C(7)	1.306(7)
Ni(1) – O(2)	2.033(4)	N(2) – C(6)	1.362(7)
Ni(1) – O(1)	2.044(4)	N(3) – C(9)	1.273(6)
Ni(1) – N(4)	2.226(4)	N(3) – C(10)	1.391(6)
Ni(1) – N(1)	2.290(4)	N(4) – C(24)	1.323(6)
O(1) – C(15)	1.301(6)	N(4) – C(17)	1.381(7)
O(2) – C(31)	1.284(6)	N(1) – C(8)	1.310(6)
Bond angles			
N(3) –Ni(1) –N(6)	176.00(18)	O(1) –Ni(1) –N(4)	88.84(14)
N(3) –Ni(1) –O(2)	94.36(16)	N(3) –Ni(1) –N(1)	76.64(18)
N(6) –Ni(1) –O(2)	81.68(18)	N(6) –Ni(1) –N(1)	103.82(17)
N(3) –Ni(1) –O(1)	81.25(17)	O(2) –Ni(1) –N(1)	90.77(15)
N(6) –Ni(1) –O(1)	98.45(16)	O(1) –Ni(1) –N(1)	157.68(16)
O(2) –Ni(1) –O(1)	93.90(15)	N(4) –Ni(1) –N(1)	94.33(14)
N(3) –Ni(1) –N(4)	106.03(17)	O(2) –Ni(1) –N(4)	159.61(17)
N(6) –Ni(1) –N(4)	77.93(18)		

Table 3.12: ***Selected hydrogen bond interactions in the complex***

D–H...A	Symmetry	Distances (Å)		Angles (◦) D–H...A
		D...A	H...A	
O(3)–H(3C)...N(5)	1/2+x,3/2–y, –1/2+z	3.015(7)	2.43	127
O(3)–H(3D)...O(1)	1–x,1–y,1–z	2.862(7)	2.18	159

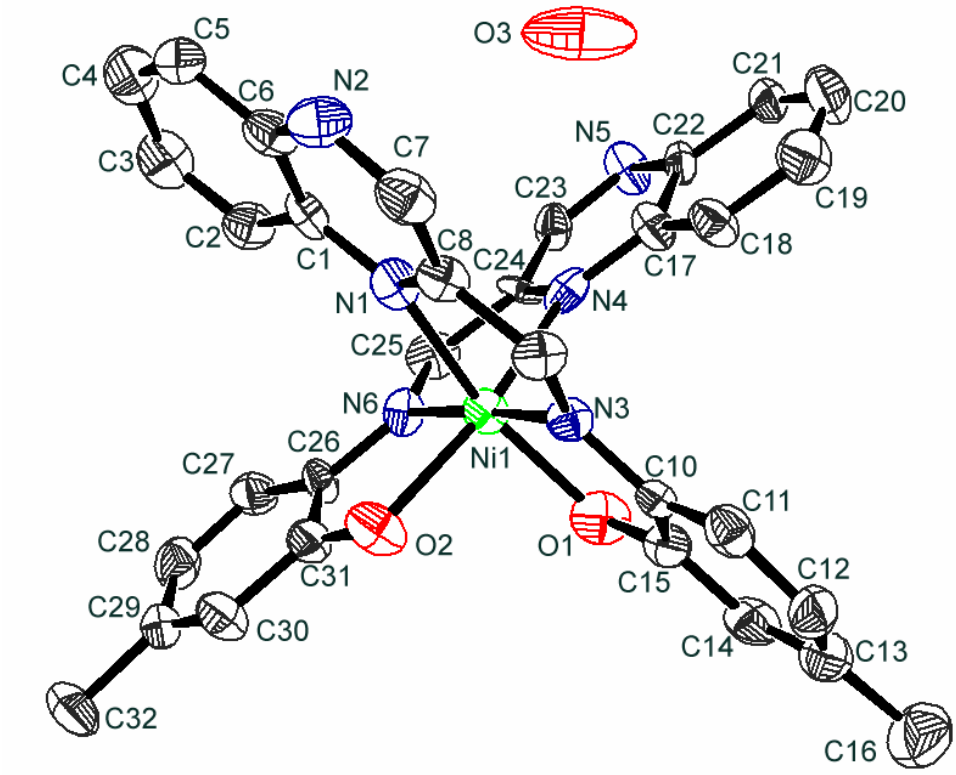

Figure 3.31: ***Ortep representation of the complex [Ni(qamp)$_2$].H$_2$O, with 50 % probability ellipsoid (Hydrogen atoms are omitted for clarity)***

3.4 CONCLUSIONS

This chapter describes the synthesis and characterizations of a new Schiff base derived from quinoxaline-2-carboxaldehyde and 2-amino-5-methylphenol,

and its complexes with Mn(II), Fe(III), Co(II), Ni(II), Cu(II) and Zn(II). Crystal structures of $[Co(qamp)_2].H_2O$ and $[Ni(qamp)_2].H_2O$ confirm the octahedral geometry of the complexes. In both the cases the unit cell contains a racemic mixture of two crystallographically independent enantiomers of the complex. The molecules exhibit a two dimensional polymeric structure parallel to [010] plane, formed by O–H…N and O–H…O intermolecular hydrogen bonding and π–π stacking interaction. We, therefore, conclude that the Schiff base can act as a good template in establishing an ordered polymeric structure. Based on the analytical and physicochemical data we have proposed the following structures for the other complexes (Figure 3.32).

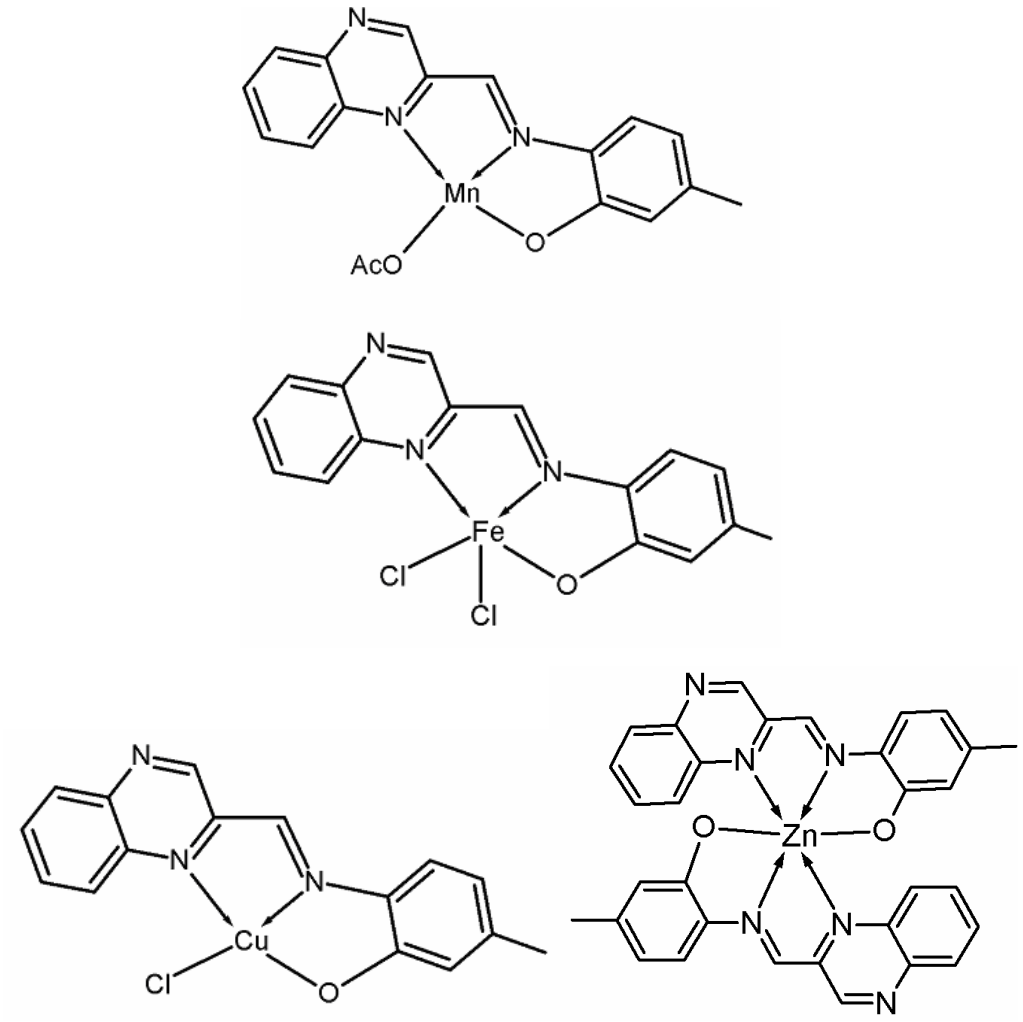

Figure 3.32: ***Proposed structures of the Schiff base complexes***

References

1. K.D. Karlin, Z. Tyeklar, *Bioinorganic Chemistry of Copper*, Chapman & Hall: New York (1993)
2. V. Arun, N. Sridevi, P.P. Robinson, S. Manju, K.K.M. Yusuff, *J. Mol. Catal. A Chem.* 304 (2009) 191.
3. K.C. Gupta, A.K. Sutar, *Coord. Chem. Rev.* 252 (2008) 1420.
4. R.I. Kureshy, N.H. Khan, S.H.R. Abdi, S.T. Patel, P. Iyer, *J. Mol. Cat. A: Chem.* 150 (1999) 163.
5. Y-B. Dong, H-Q. Zhang, J-P. Ma, R.-Q. Huang, *Cryst. Growth Des.* 5 (2005) 1857.
6. A.K. Ghosh, D. Ghoshal, J. Ribas, G. Mostafa, N.R. Chaudhuri, *Cryst. Growth Des.* 6 (2006) 36.
7. P. Phuengphai, S. Youngme, P. Kongsaeree, C. Pakawatchai, N. Chaichit, S.J. Teat, P. Gamez , J. Reedijk, *CrystEngComm* 11 (2009) 1723.
8. P.A. Vigato, S. Tamburini, *Coord. Chem. Rev.* 248 (2004)1717.
9. A. Vogler, H. Kunkely, *Coord. Chem. Rev.* 177 (1998) 81.
10. M. Prabhakar, P.S. Zacharias, S.K. Das, *Inorg. Chem.* 44 (2005) 2585.
11. P.P. Hankare, S.S. Chavan, *Synth. React. Inorg. Met.-Org. Chem.* 33 (2003) 423.
12. N. Raman, A. Kulandaisamy, K. Jeyasubramanian, *Synth. React. Inorg. Met.-Org. Chem.* 31 (2001) 1249.
13. A.A. Soliman, G.G. Mohamed, *Thermochim. Acta* 421 (2004) 151.
14. PhD Thesis, S. Mayadevi, *Studies on some transition metal complexes of the Schiff bases derived from quinoxaline-2-carboxaldehyde*, Cochin University of

Science and Technology (1998).

15. W.J. Geary. *Coord. Chem. Rev*. 7 (1971) 8.

16. M-A. Kopf, D. Varech, J-P. Tuchagues, D. Mansuy, I. Artaud, *J. Chem. Soc*., *Dalton Trans*. (1998) 991

17. T. Sakai, Y. Ohgo, A. Hoshino, T. Ikeue, T. Saitoh, M. Takahashi, M. Nakamura, *Inorg. Chem.* 43 (2004) 5034.

18 F.A. Cotton, G. Wilkinson, C.A. Murillo, M. Bochmann, *Advanced Inorganic Chemistry*, sixth ed., Wiley, New York (1999).

19 S. Mayadevi, P.G. Prasad, K.K.M. Yusuff, *Synth. React. Inorg. Met.-Org. Chem.* 33 (2003) 481.

20 K.S. Bose, B.C. Sharma, C.C. Patel, *J. Inorg. Nucl. Chem.* 32 (1970) 1742.

21 L.J. Bellamy, *The infra-red spectra of complex molecules*, London:Methuen (1956).

22 D.N. Sathyanarayana, *Vibrational spectroscopy: Theory and applications*, New Age International Publishers, New Delhi (2004).

23 M.A. Neelakantan, S.S. Marriappan, J. Dharmaraja, T. Jeyakumar, K. Muthukumaran, *Spectrochim. Acta A* 71 (2008) 628.

24 J.C. Bailar, H.J. Emeleus, R. Nyholm, A.F. Trotman-Dickenson, *Comprehensive Inorganic Chemistry*, Vol. 3, Pergamon Press (1975).

25 A.B.P. Lever, *Inorganic Electronic Spectroscopy*, 2nd Edn, Elsevier, Amsterdam (1984).

26 R.L. Martin, A.H. White, *Inorg. Chem.* 6 (1967) 712.

27 A.D. Naik, S.M. Annigeri, U.B. Gangadharmath, V.K. Revankar, V.B. Mahale. *Spectrochim. Acta A* 58 (2002) 1713.

28 S. Hong, X. Liang, H. Fang, X. Zhan, Z. Zhou, L. Chen, Y. Cai. *Transition Met*

Chem. 34 (2009) 115.

29 T.A. Khan, S.Naseem, S.N. Khan, A.U. Khan, M. Shakir, *Spectrochim. Acta A* 73 (2009) 622.

30 D.J.E. Ingram, *Spectroscopy at Radio and Microwave frequencies*, 2nd ed., Butterworth, London (1967).

31 D. Kivelson, R. Neiman, *J. Chem. Phys.* 35 (1961) 149.

32 K. Sundaravel, E. Suresh, M. Palaniandavar, *Inorg. Chim. Acta* 362 (2009) 199.

33 P.F. Rapheal, E. Manoj, M.R.P. Kurup, *Polyhedron* 26 (2007) 818.

34 N.B.M. ElMkacher, M. Rzaigui, F. Bouachir. *Acta Cryst*. E64 (2008) o271.

35 M. Koikawa, M. Ohba, T. Tokii, *Polyhedron* 24 (2005) 2257.

36 P. Mukherjee, M.G.B. Drew, C.J.Gomez-Garcia, A. Ghosh, *Inorg. Chem.* 48 (2009) 5848.

37 B.A. Bovenzi, G.A. Pearse, *J. Chem. Soc., Dalton Trans.* (1997) 2793.

38 A. Lalehzari, J. Desper, C.J. Levy, *Inorg. Chem.* 47 (2008) 1120.

39 H.C. Aspinall, *Chem. Rev.* 102 (2002) 1807.

40 C. Piguet, G. Bernardinelli, G. Hopfgartner, *Chem. Rev.* 97 (1997) 2005.

41 S.D. Reid, A.J. Blake, W. Köckenberger, C. Wilson, J.B. Love, *Dalton Trans.* (2003) 4387.

42 M. Seitz, A. Kaiser, S. Stempfhuber, M. Zabel, O. Reiser, *J. Am. Chem. Soc.* 126 (2004) 11426.

43 M. Albrecht, *Chem. Rev.* 101 (2001) 3457.